

# Hydrothermal fabrication of WO<sub>3</sub>-modified TiO<sub>2</sub> crystals and their efficiency in photocatalytic degradation of FCF

C. P. Sajan<sup>1</sup> · A. Naik<sup>2</sup> · H. N. Girish<sup>3</sup>

Received: 28 February 2016/Revised: 31 October 2016/Accepted: 26 December 2016/Published online: 30 January 2017  
© Islamic Azad University (IAU) 2017

**Abstract** WO<sub>3</sub>-modified TiO<sub>2</sub> polyscale crystals were fabricated successfully using the hydrothermal technique. The as-prepared samples were characterized using powder X-ray diffraction, scanning electron microscopy, Fourier transform infrared spectroscopy, photoluminescence spectroscopy and UV–vis spectroscopy. The photocatalytic application of these synthesized samples was confirmed by photocatalytic degradation of fast green dye solution under sunlight and UV irradiation. The degradation efficiency was analyzed by measuring the parameters such as percent transmittance, chemical oxygen demand and percent decomposition of the dye solution. It was noted that the photodegradation efficiency of the samples varies with added amounts of WO<sub>3</sub> content. The highest photodegradation efficiency was obtained using 2WT sample where the pace of decomposition was 70.5% under UV light and 81.3% under sunlight.

**Keywords** Photocatalysis · Hydrothermal · Fast green dye

---

Editorial responsibility: Agnieszka Galuszka.

**Electronic supplementary material** The online version of this article (doi:10.1007/s13762-016-1239-1) contains supplementary material, which is available to authorized users.

---

✉ C. P. Sajan  
sajan.saj@rediff.com

<sup>1</sup> Department of Studies in Environmental Science, University of Mysore, Manasagangothri, Mysore 570 006, India

<sup>2</sup> Maharshi Dayanand College of Arts, Science and Commerce, Mumbai 400012, India

<sup>3</sup> Department of Studies in Earth Science, University of Mysore, Manasagangothri, Mysore 570 006, India

## Introduction

Broadly speaking, the dye can be described as a coloring substance that has an affinity to the substrate to which it is being applied (Brown et al. 1981). In recent years, dyes are considered as one of the major industrial pollutants and water contaminants. The concentration of organics present in industrial effluents and the stability of modern synthetic dyes are very high which makes the conventional biological treatment method ineffective for complete color removal and degradation of organics (Souther and Alspaugh 1957; Hamza and Hampda 1980). Dyes have been identified as problematic compounds in textile wastewaters as they are water soluble and cannot be easily removed by conventional aerobic biological wastewater treatment systems. Advanced oxidation processes are of ample interest, currently for the effective oxidation of a wide variety of organics and dyes (Kang and Hoffmann 1998; Boye et al. 2002). Among them, top priority goes to semiconductor-assisted photocatalytic degradation. Advanced oxidation processes using semiconductor photocatalysis have been considered as a promising technique for decontamination, purification and/or deodorization of polluted water (Griboval et al. 1999; Rajeshwar et al. 2008; El Saliby et al. 2012; Jung et al. 2013; Naeem and Ouyang 2013; Adhikari et al. 2015; Stock et al. 2000). Semiconductor-based photocatalysts have been extensively studied due to their excellent photocatalytic activity and its potential applications toward photo-splitting of water, photocatalysis, photonic devices, carbon reduction, hydrogen production and sensors (Ong et al. 2014, 2015, 2016; Du et al. 2015). Most of the photocatalytic studies use either synthetic or commercial TiO<sub>2</sub> as the photocatalyst (Grzechulska and Morawski 2002; Noorjahan et al. 2004). Titania is an

important catalytic material, not simply because of its effectiveness in photoassisted reaction (Anpo 1989), but likewise because it heightens the natural action and selectivity of transition and noble metals when used as a support (Wainwright and Foster 1979; Vannice 1982; Wachs et al. 1985; Kung et al. 1989; Li et al. 2015; Ong et al. 2015). Recently, material scientists have given much attention in fabricating of modified TiO<sub>2</sub> crystals and their application in environmental remediation and energy conversion. TiO<sub>2</sub> coupled with metal oxides has been reported to show an enhance photocatalytic activity (Sajan et al. 2010; Ashok et al. 2016). Among metal oxides, WO<sub>3</sub> is considered as one of the important candidates, due to its structural flexibility and its intercalated states of cation (Nah et al. 2008; Su et al. 2011). The band gap energy of WO<sub>3</sub> varies from 2.6 to 3.0 eV and TiO<sub>2</sub> varies from 3.0 to 3.2 eV; when these metal oxides are coupled, the band gap difference between these two semiconductors reduces the recombination of charge carriers, which leads to the formation of more photogenerated electrons which further participate in the photocatalytic reaction. Furthermore, WO<sub>3</sub> when used as a coupling material with TiO<sub>2</sub>, the electro-chromic property of WO<sub>3</sub> makes the composite material more flexible such that the composite can be used under both UV irradiation and visible light. Even the better photocatalytic activity can be expected when exposed to visible light compared to UV light (Leghari et al. 2011; Su et al. 2011). In the present study, we report one of the simplest routes for the fabrication of WO<sub>3</sub>-modified TiO<sub>2</sub> polyscale crystals using hydrothermal technique and its application in the photodegradation of fast green dye.

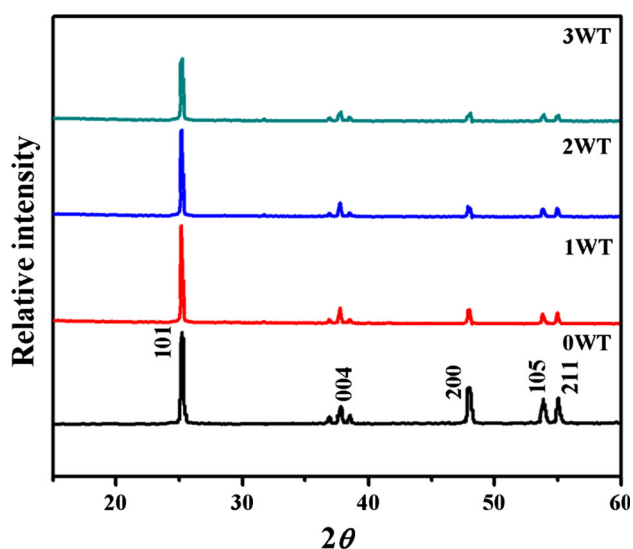


**Fig. 1** XRD powder diffraction pattern of WO<sub>3</sub>-modified TiO<sub>2</sub> polyscale crystals

## Materials and methods

### Materials

Titanium sulfate (TiSO<sub>4</sub>), tungsten trioxide (WO<sub>3</sub>) and hydrofluoric acid (HF) were supplied from Loba Chemicals Co. Ltd and Qualignes Co. Ltd. All the reagents were analytical grade and used without further purification. Distilled water was used for post-treatment processes.

### Hydrothermal synthesis of WO<sub>3</sub>-modified TiO<sub>2</sub> polyscale crystals

In the present work, commercial TiSO<sub>4</sub> was used as starting material. 4.3 gm of TiSO<sub>4</sub> was taken in a Teflon liner to which 25 ml of ethanol was added and stirred for 2 h till a clear solution is formed. 0.5 ml of HF followed by 0.5 ml of distilled water was added for effective hydrolyzing of TiSO<sub>4</sub> to TiO<sub>2</sub> maintaining the percent fill of 40%. To this solution, WO<sub>3</sub> was added in different weight ratio and kept stirred using a magnetic stirrer for another 1 h. The Teflon liner was closed and placed in an autoclave, and heated at the 200 °C for 24 h. For comparison, the experiment was carried in the absence of both HF and water separately. After the experimental run, the autoclave was quenched using an air jet to arrest the temperature at which the crystals are formed and the liner was taken out. The sample inside the liner was separated from the solution and washed with the double-distilled water till the pH become neutral, and then ultrasonicated. The product extracted was centrifuged to remove undesired components and dried at a temperature of 35–40 °C in a dust free environment. The extracted samples were labeled based on the ratio of WO<sub>3</sub>:TiO<sub>2</sub> as 0WT, 1WT, 2WT and 3WT, where 0, 1, 2 and 3 represents the weight% of WO<sub>3</sub> added. The blank WO<sub>3</sub> sample was considered as W.

The as-prepared samples were used for the photocatalytic degradation of fast green dye. In the photocatalytic degradation of the fast green dye, a known volume of the dye solution (50 ml) of known concentration ( $1 \times 10^{-5}$ ) was held in a beaker. To this, a known amount of catalyst was added. For comparison, the experiment was extended out under both UV and sunlight. The samples were kept in the UV chamber (Sankyo, Denki, Japan, 8W) which serves

**Table 1** Cell parameters of WO<sub>3</sub>-modified TiO<sub>2</sub> polyscale crystals

Compound	<i>a</i> -axis Å	<i>b</i> -axis Å	<i>c</i> -axis Å	Cell volume Å <sup>3</sup>
0WT	3.78	3.78	9.51	136.88
1WT	3.7885	3.7885	9.5217	136.66
2WT	3.7890	3.7890	9.5206	136.68
3WT	3.7907	3.7907	9.5212	136.81

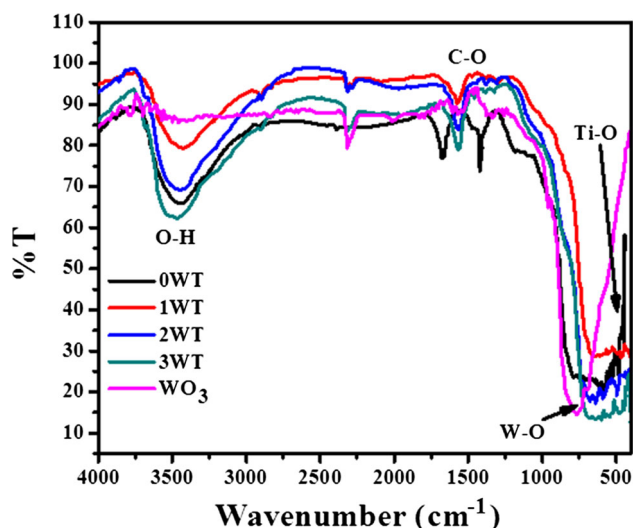


**Fig. 2** FTIR spectra of  $\text{TiO}_2$ ,  $\text{WO}_3$  and  $\text{WO}_3$ -modified  $\text{TiO}_2$  polyscale crystals

as UV source. The distance between the UV light and dye solution was 18 cm. The intensity of sunlight and UV light was estimated by photolysis of uranyl oxalate. It was calculated that the intensity of sunlight was  $6.722 \times 10^{16}$  quanta/s, and the intensity of UV was  $2.375 \times 10^{15}$  quanta/s. 2–3 ml of the sample exposed to light was taken and centrifuged for 4–5 min at 1000 rpm and then used to measure the percentage transmission (%T) at 540 nm using a spectrophotometer. Chemical oxygen demand (COD) was estimated before and after the treatment (using the  $\text{K}_2\text{Cr}_2\text{O}_7$  oxidation method). The photodegradation efficiency of the dye solution was estimated utilizing the equation,

$$\begin{aligned} &\text{Photodegradation or decomposition} \\ &= \frac{\text{Initial}_{\text{COD}} - \text{Final}_{\text{COD}}}{\text{Initial}_{\text{COD}}} \times 100 \end{aligned}$$

## Results and discussion

### Instrumentation and characterization

The X-ray powder diffraction (XRD) pattern of the synthesized compound was recorded using Rigaku Miniflex X-ray diffractometer (Model IGC2, Rigaku Co. Ltd, Japan). The  $2\theta$  range was set between  $10^\circ$  and  $80^\circ$ . The identification of the crystalline phase was accomplished by comparing with JCPDS using PCPDF Win version 2.01, and the cell refinement was done using chek cell software. The Fourier transform infrared spectrometry (FTIR) spectra were recorded using JASCO-460 Plus, Japan. The morphology of the samples extracted was characterized using a high-resolution scanning electron microscope (SEM) TSL MSC-2200. Transmission electron microscopy

(TEM) and high-resolution transmission electron microscopy (HRTEM) analyses were conducted on a JEM-2100F electron microscope (JEOL, Japan) using a 200 kV accelerating voltage. UV–visible spectrophotometer (UV-2550, Shimadzu, Japan) was utilized to record UV–visible absorbance spectra for the dry-pressed samples using  $\text{BaSO}_4$  as a touchstone. Photoluminescence (PL) spectra were measured at room temperature on a Fluorescence Spectrophotometer (F-7000, Hitachi, Japan). %T of dye solution before and after photodegradation was studied using a spectrophotometer (Model: Minispec SL 171, Elico, India).

### X-ray diffraction studies of $\text{WO}_3$ -modified $\text{TiO}_2$ polyscale crystals

The powder X-ray diffraction patterns of the as-prepared samples are shown in Fig. 1. The identification of crystalline phase of these samples was done by comparison with JCPDS file (PCPDFWIN-2.01). The X-ray patterns match with PDF: 83-2256 belonging to an I4/MCM space group. All the diffraction peaks of the synthesized samples match with the standard data of PDF: 83-2256. However, it was also observed that with an increase in wt% of  $\text{WO}_3$  the intensity of (101) planes tends to decrease signifying the deposition of  $\text{WO}_3$  on to (101) planes. The (101) facet of  $\text{TiO}_2$  is more reductive and has the affinity to gain more electrons than (001) facet (Xiong and Zhao 2012), possibly due to which the  $\text{WO}_3$  gets deposited onto the (101) facet. Meanwhile, there is a slight shift in peak intensities suggesting the effect of doping  $\text{WO}_3$  into  $\text{TiO}_2$  lattice. Furthermore, we noticed that no peaks related to  $\text{WO}_3$  were witnessed, confirming the effective doping of dopants into the crystal lattice. In order to know the change in crystal structures after doping, cell refinement was done using chek cell software. The cell parameters obtained after elaboration of these samples are presented in Table 1. Table 1 shows that, on doping the cell volume reduces, the reduction in cell volume is due to the smaller ionic radii of  $\text{W}^{6+}$  (ionic radii of  $\text{W}^{6+}$  is 60 pm and  $\text{Ti}^{4+}$  60.5 pm) which might have replaced  $\text{Ti}^{4+}$ . It was likewise discovered that the cell volume gradually increases with an increase in dopant concentration. XRD pattern and Table 1 confirm the effective deposition and doping of  $\text{W}^{6+}$ .

### FTIR studies of prepared $\text{WO}_3$ -modified $\text{TiO}_2$ polyscale crystals

The FTIR spectral studies of  $\text{WO}_3$ ,  $\text{TiO}_2$  and  $\text{WO}_3$ -modified  $\text{TiO}_2$  polyscale crystals were performed to support the existence of tungsten in the samples synthesized



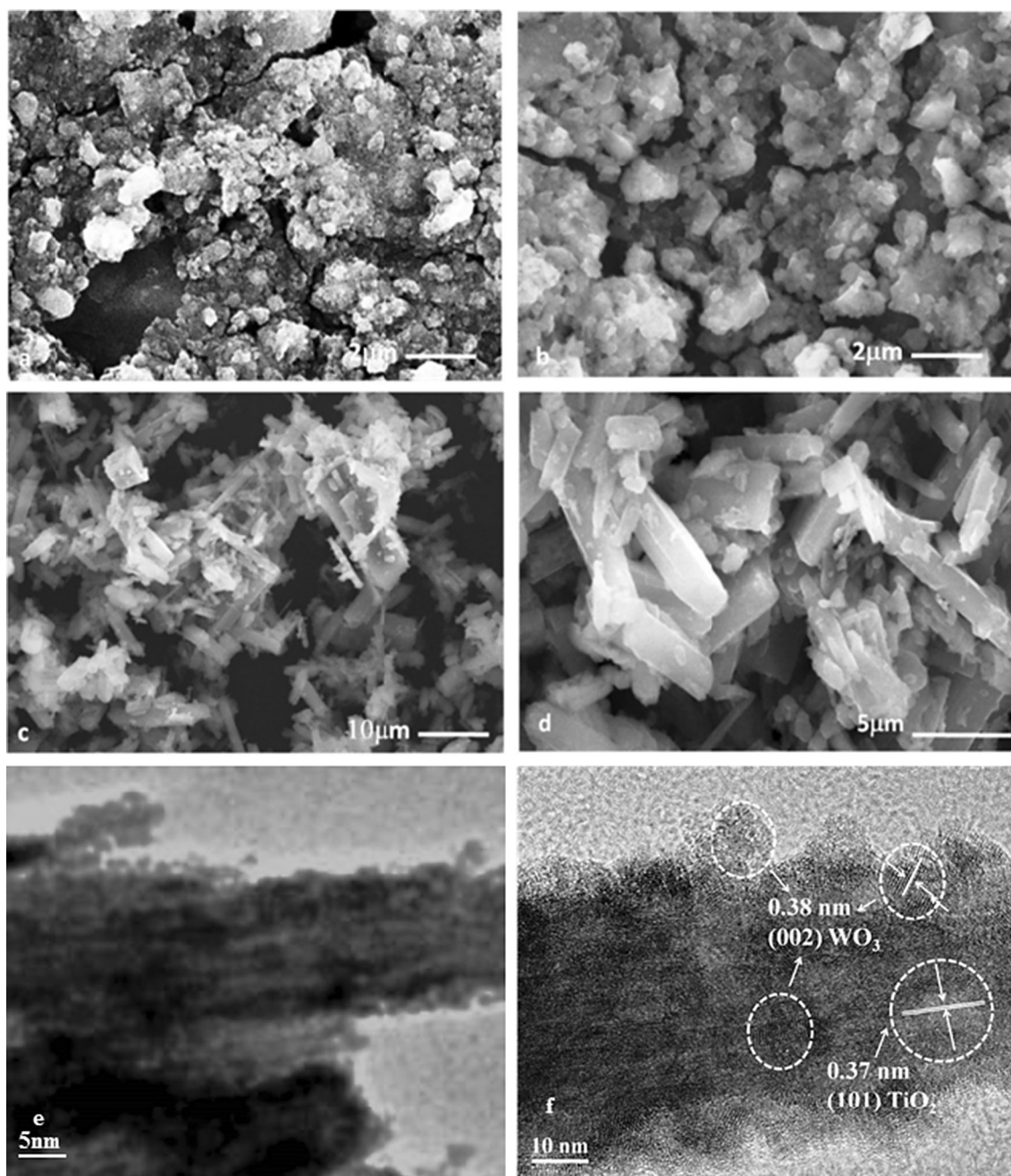


**Fig. 3** SEM and TEM images of  $\text{WO}_3$ -modified  $\text{TiO}_2$  polyscale crystals **a** synthesized in the absence of HF, **b** synthesized in the absence of  $\text{H}_2\text{O}$ , **c** and **d** synthesized in the presence of both HF and

$\text{H}_2\text{O}$  (2WT) **e** TEM image of 3WT sample and **f** HRTEM image showing lattice fringes of 3WT sample

(Fig. 2). The peaks around the region  $3400\text{ cm}^{-1}$  in the spectra represent an O–H stretching (Che Ramli et al. 2014), which is originated due to the addition of water for hydrolyzing  $\text{TiSO}_4$  to  $\text{TiO}_2$ . The band within the region  $1600$  and  $2360\text{ cm}^{-1}$  is attributed to the C–O stretching, caused by the absorption of atmospheric  $\text{CO}_2$  on the metal

cations (Liao et al. 2002). The region between  $470$  and  $500\text{ cm}^{-1}$  clearly represented the Ti–O stretch (Nolan et al. 2009). The band in the region  $683$ – $828\text{ cm}^{-1}$  corresponds to the W=O stretching of tungsten oxide complex confirming the presence of W (Safaei and Mohebbi 2016).

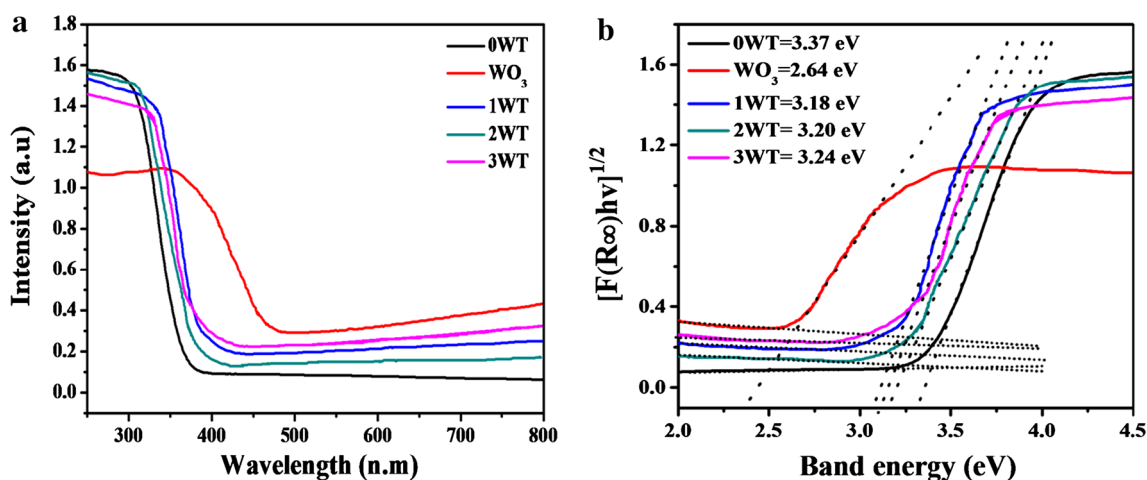


Fig. 4 UV-vis absorption spectra of  $\text{WO}_3$ -modified  $\text{TiO}_2$  polyscale crystals

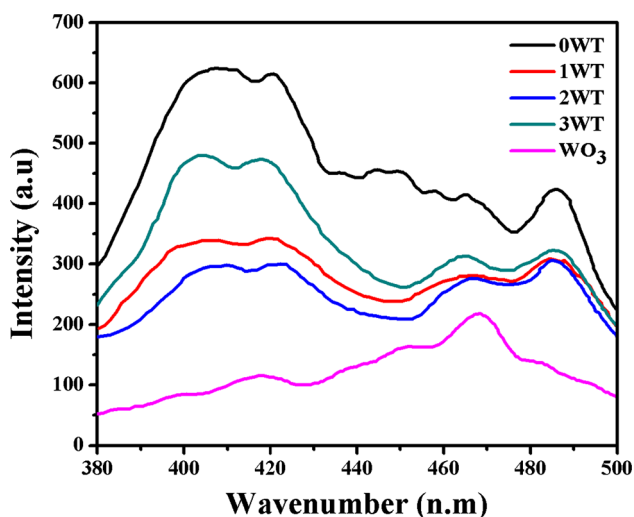


Fig. 5 PL spectra of  $\text{WO}_3$ -modified  $\text{TiO}_2$  polyscale crystals

#### SEM and TEM studies of $\text{WO}_3$ -modified $\text{TiO}_2$ polyscale crystals

The morphology and the structural features of the synthesized samples were analyzed through SEM and TEM micrographic studies (Fig. 3). In the absence of HF, botryoidal or globular type of crystals having hemispherical masses was observed. However, when HF was added in the absence of  $\text{H}_2\text{O}$ , crystal-like structures with irregular shape and size were observed. In the bearing of both  $\text{H}_2\text{O}$  and HF well-defined, agglomerated, polyscale crystals ranging from 1 to  $>10\ \mu\text{m}$  were observed which are tabular in form and hexagonal in shape. Onto these crystals, depositions of small crystals were observed. These small tiny fragments onto  $\text{TiO}_2$  polyscale crystal structure might be  $\text{WO}_3$  particles. The HRTEM image (Fig. 3f) further reveals that the lattice fringes are parallel to the growth direction of the crystals. The lattice spacing measured for the crystalline planes having 0.37 nm corresponds to (101) plane of  $\text{TiO}_2$

polyscale crystals, and the same plane was observed in the XRD pattern where the (101) plane was prominent. Lattice spacing measured from the crystalline plane having 0.38 nm corresponds to (002) plane of  $\text{WO}_3$ . The deposition of  $\text{WO}_3$  onto  $\text{TiO}_2$  polyscale crystals forms an intimate contact, which facilitates the electron transfer from  $\text{TiO}_2$  crystals to  $\text{WO}_3$  particles during the photoexcitation process. Based on the SEM and HRTEM studies, one can clearly conclude that both  $\text{H}_2\text{O}$  and HF when added in a right proportion play a crucial role in the processing of  $\text{WO}_3$ -modified  $\text{TiO}_2$  polyscale crystals with well-defined morphology at present set PT condition.

#### UV-vis diffuse reflectance spectra

The UV absorption spectral studies were carried out for the synthesized samples (Fig. 4). It was observed that with an increase in  $\text{WO}_3$  content, there is a significant increase in the absorption of the samples, above wavelength around 387 nm which is ascribed to the band gap absorption of  $\text{TiO}_2$  (3.2 eV). However, with a change in  $\text{WO}_3$  concentration, there is an increase in redshift absorption of the samples which further confirms the effective deposition of  $\text{WO}_3$  and doping of  $\text{W}^{6+}$  into  $\text{TiO}_2$  lattice (Sayama et al. 2000; Wang and Lewis 2005). Among the synthesized samples, 2WT sample shows an enhanced redshift absorption and visible light absorption ranging from 387 to 800 nm indicating that 2WT-modified  $\text{TiO}_2$  polyscale crystal sample might show higher photocatalytic activity than other samples under visible light irradiation. Furthermore, it was observed that there is an increase in absorbance in the visible light region with an increase in  $\text{WO}_3$  content. The increase in absorbance further leads to the modification of electron-hole pair formation upon irradiation which are formed as a result of stronger background absorption contributed from  $\text{WO}_3$ . The band gap energy of the crystals synthesized was estimated using

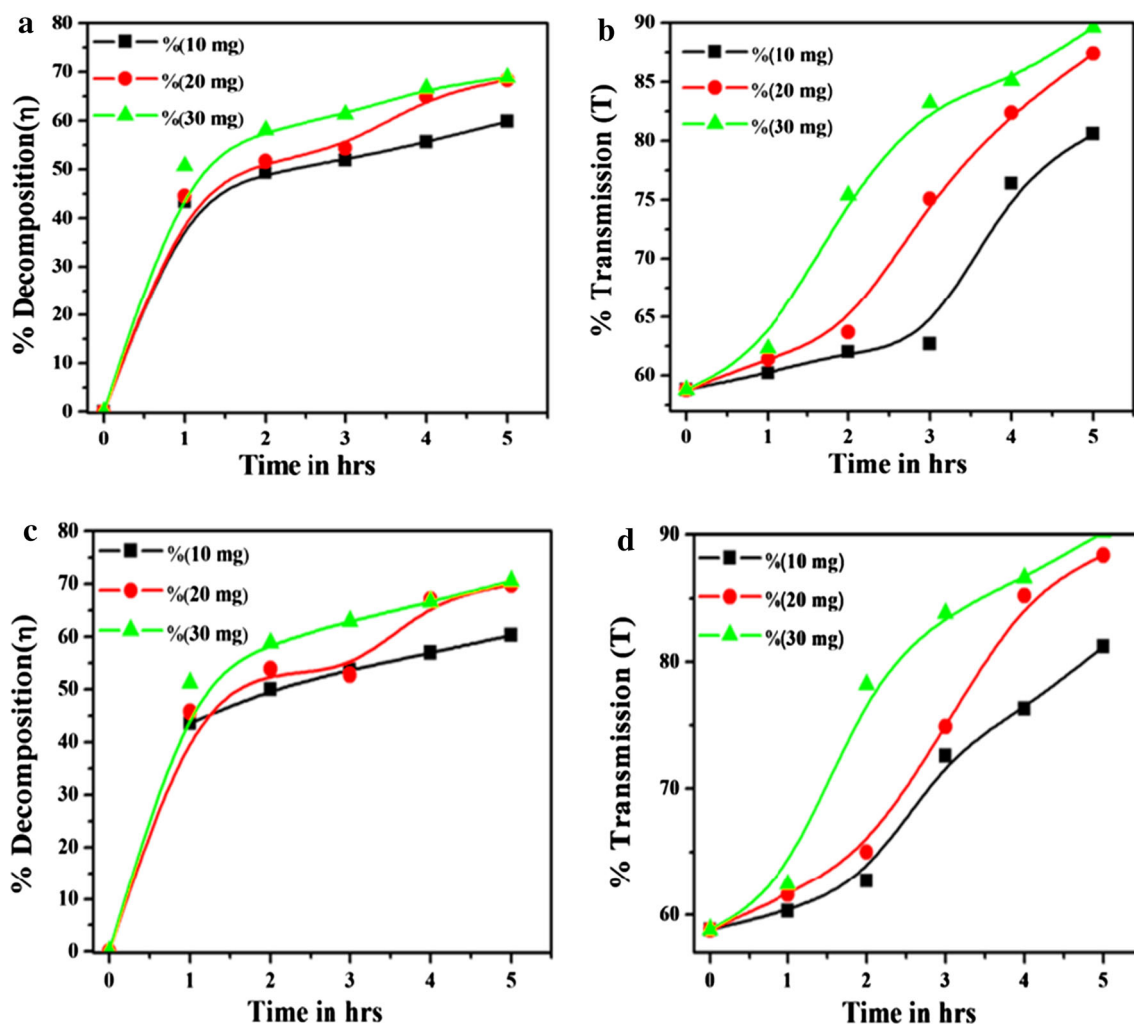


**Fig. 6** Graphical representation of increase in % decomposition and % transmission **a, b** under UV light using 1WT, **c, d** % decomposition and % transmission under sunlight using 1WT

Tauc plot and the extrapolation of the linear slope of photon energy (Fig. 4b). It was observed that the band gap of  $\text{WO}_3$  and  $\text{TiO}_2$  polyscale crystals were 2.64 and 3.37 eV, respectively. Band gap studies further confirmed that the deposition of  $\text{WO}_3$  further leads to the decrease in the band gap of  $\text{TiO}_2$  crystals with respect to the amount  $\text{WO}_3$  deposited. In the present work, the band gap of the  $\text{TiO}_2$  has reduced from 3.37 to 3.18 eV.

#### PL spectral studies

The efficiency of charge carrier trapping, immigration and transfer of electrons can be effectively analyzed using PL spectral studies. Deposition of  $\text{WO}_3$  and doping of  $\text{W}^{6+}$  onto  $\text{TiO}_2$  polyscale crystals has a significant effect on the PL intensity (Fig. 5). The intensity of PL decreases with increasing  $\text{WO}_3$  content and reaches the lower degree when  $\text{WO}_3$  content reached 2 wt%. Nevertheless, when the  $\text{WO}_3$  content was increased to 3 wt%, the intensity of PL begins to

grow. It is well recognized that lesser recombination results in a reduction of PL intensity and increase the photocatalytic activity of the semiconductor. This is because PL emission is produced from the recombination of photogenerated electrons and holes. As a resolution, the high peak intensity results in higher recombination of electron and holes having lower photocatalytic activity. In the present study, 2WT sample shows lower intensity compared to the other samples, signifying that deposition of  $\text{WO}_3$  onto  $\text{TiO}_2$  polyscale crystals has a major effect in reducing the recombination of electrons and holes and the possibility of showing high photocatalytic activity. The rapid electron transfer between  $\text{WO}_3$  and  $\text{TiO}_2$  crystals results in higher quantum efficiency, thereby supplying more photogenerated electrons. When  $\text{TiO}_2$  polyscale crystals were deposited with  $\text{WO}_3$  above 2 wt%, the increased amount of  $\text{WO}_3$  particles serves as charge recombination centers, which further increase the intensity of the PL spectra, thereby leading to the reduction of photocatalytic efficiency.



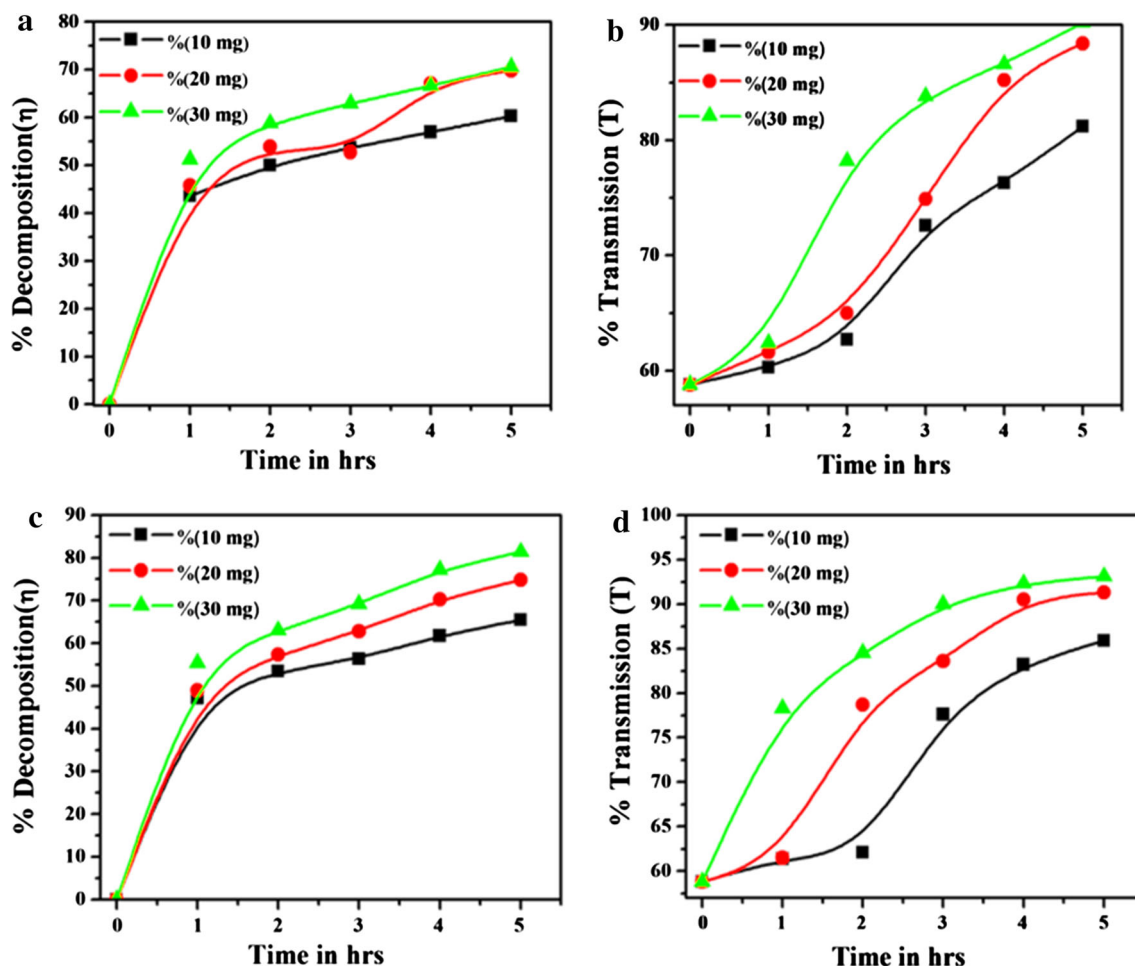


**Fig. 7** Graphical representation of increase in % decomposition and % transmission **a, b** under UV light using 2WT, **c, d** % decomposition and % transmission under sunlight using 2WT

#### Photodegradation studies of fast green dye using $WO_3$ -modified $TiO_2$ polyscale crystals

It is well known that the photodegradation process assisted by a semiconductor depends on various parameters such as nature and concentration of the organic substrate, concentration and type of the semiconductor, light source and intensity, pH and temperature (Ferraz et al. 1999). In the present work, the photodegradation of fast green dye was done using  $WO_3$ -modified  $TiO_2$  polyscale crystals of different concentration under UV light and sunlight. To obtain an optimum condition at which photodegradation of FCF is the maximum, the degradation process was carried out using a different weight of the synthesized photocatalysts with respect to time. The growth in the % decomposition and % transmission illustrates the destruction of dye particles. Figures 6, 7, 8 represent the increase in % decomposition and % transmission under different light source using 1WT, 2WT and 3WT. The results obtained are given in Table 1S–6S (supplementary information). Figures 6, 7,

8 show that with an increase in the catalyst content the photodegradation efficiency increases (it should be noted that beyond 30 mg of the samples the dye solution turned turbid and so no attempt on the photocatalytic degradation of dye beyond 30 mg was made). The above estimation led to a conclusion that the optimum amount of the sample/ photocatalysts that has to be used in the present study is 30 mg. The degradation profile for the degradation of FCF using the W, 0WT, 1WT, 2WT and 3WT samples is given by  $C/Co$ , where ‘C’ stands for the initial ‘T%’ of the dye solution and ‘Co’ represents final ‘T%’ obtained after exposed to UV/sunlight at different time intervals and at the initial time, respectively. It is clearly evident from the degradation profile (Fig. 9a, b) that the degradation of FCF is higher when 2WT sample is used which further increases with respect to time.

The photocatalytic efficiency of the prepared samples was estimated based on the reaction kinetics of the photocatalytic degradation of the FCF dye solution. The reaction kinetics for the photocatalytic degradation of the



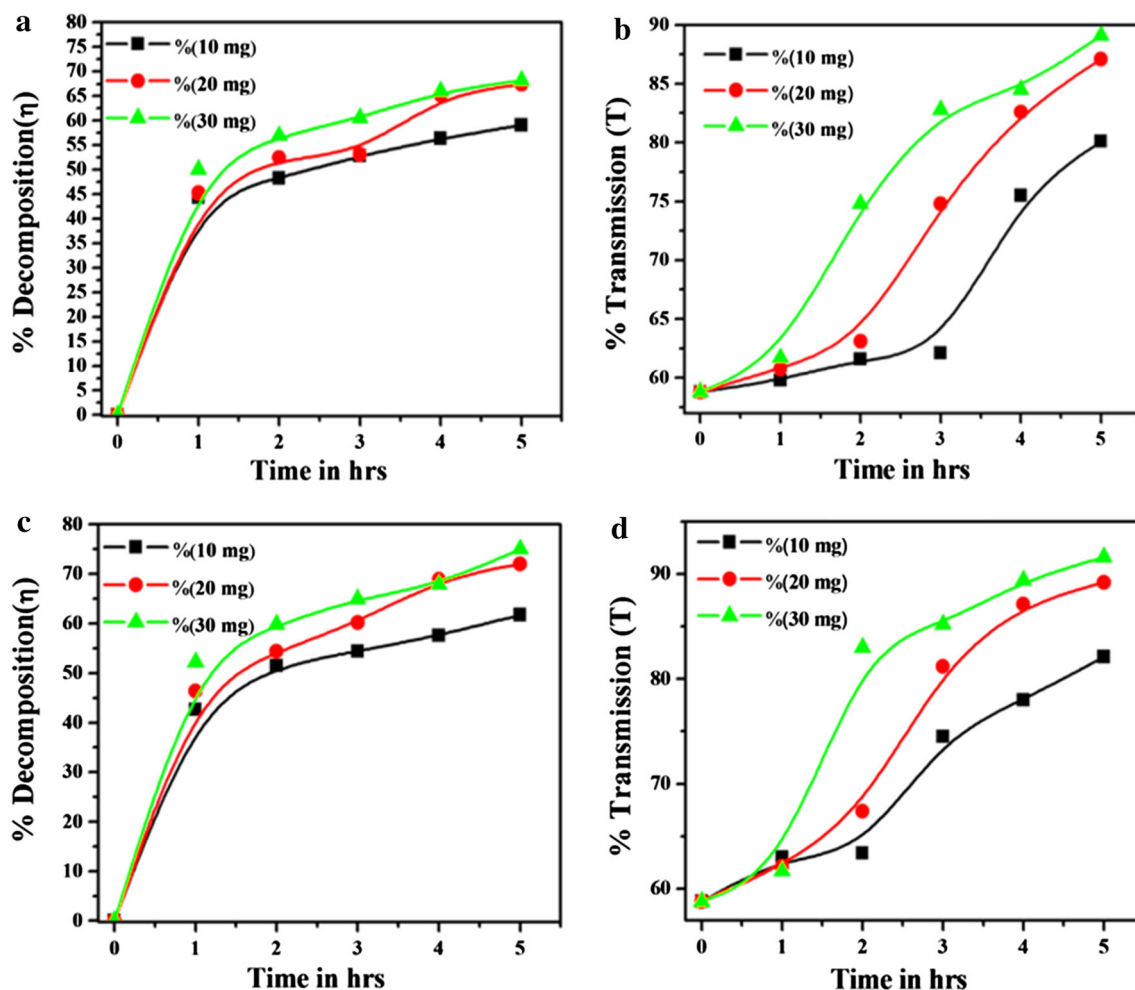


**Fig. 8** Graphical representation of increase in % decomposition and % transmission **a, b** under UV light using 3WT, **c, d** % decomposition and % transmission under sunlight using 3WT

FCF dye solution was estimated using the equation  $-\ln(C/C_0) = kt$ , where  $C$  is the concentration of dye solution after exposing to UV/sunlight at the time ( $t$ ),  $C_0$  is the initial concentration, ' $k$ ' is the obvious reaction rate constant and ' $t$ ' is the reaction time. The kinetic rate constant was obtained by plotting a linear plot of  $-\ln(C/C_0)$  verses ' $t$ ' (Fig. 9c, d). The rate constant ' $k$ ' in  $\text{min}^{-1}$  is obtained by drawing a slope. The photodegradation of FCF under both UV and sunlight is in agreement with the pseudo-first-order kinetic reaction and is represented by the straight-line fitting. The obvious reaction rate constant  $k$  ( $\text{min}^{-1}$ ) of different samples for the photodegradation of FCF was calculated from the slope of the kinetic plot which is given in Fig. 10a, b. The rate constant obtained and the correlation coefficient extracted from the plot is tabulated in Table 2.

Furthermore, to know the best efficiency among the samples synthesized a comparison study on the photocatalytic decomposition of FCF was performed (Fig. 10c). Maximum efficiency of 81% of decomposition rate was observed using 2WT under sunlight, which is consonant with the UV-*vis* and PL spectral studies. The presence of  $\text{WO}_3$  might have changed the band gap of the photocatalyst by acting either as a reinforcement or as a dopant and also has favored in reducing the electron-hole recombination, which in turn has resulted in raising the efficiency of the photodegradation of fast green dye. The % decomposition performance in a cycling photocatalytic run was performed to know the stability of 2WT. This sample showed good photocatalytic property for three cycles whose efficiency after three cycles decreased to 64% under visible light. The stability and recycling





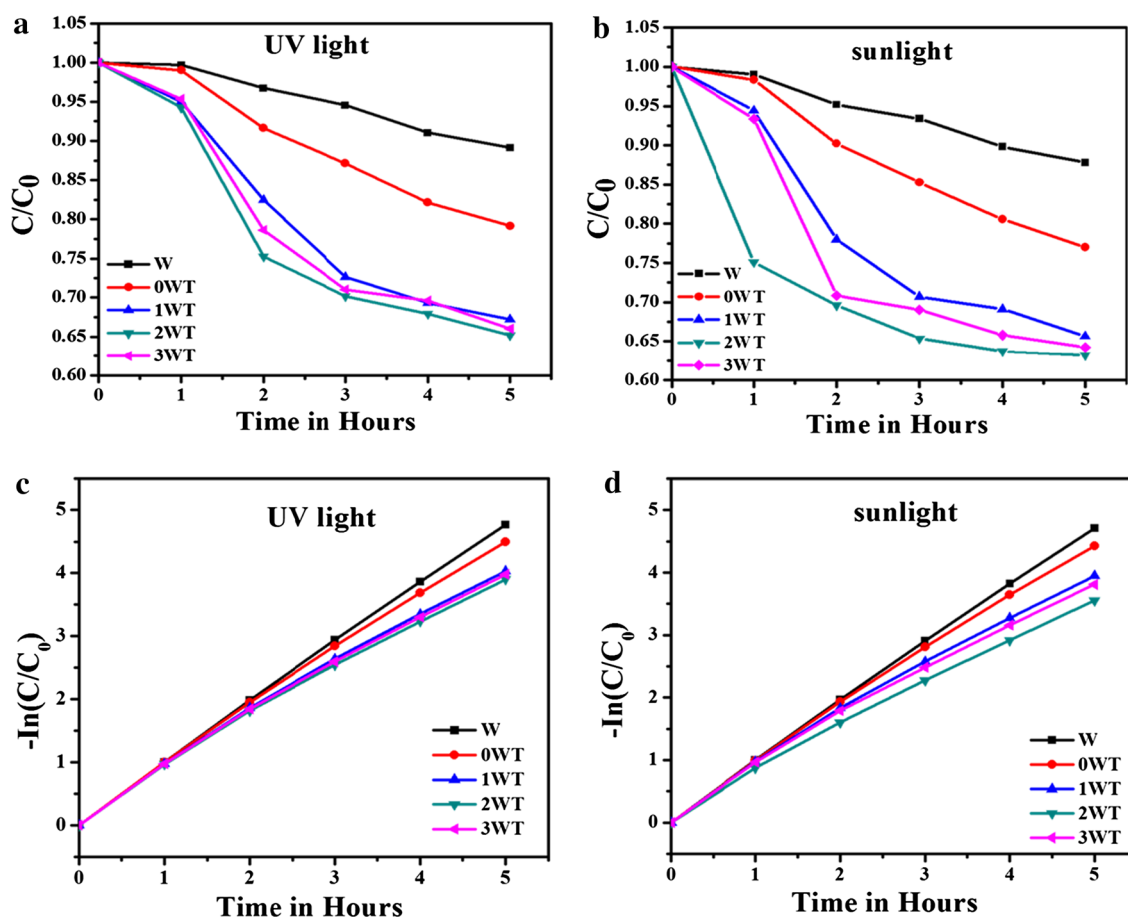


**Fig. 9** a, b Degradation profile of FCF under UV light and sunlight using W, 0WT, 1WT, 2WT and 3WT samples. c, d Kinetic studies of FCF degradation under UV light and sunlight using W, 0WT, 1WT, 2WT and 3WT samples

performance of photocatalysts are important factors for virtual applications. Not much difference was noted in the decay rate of FCF after three cycles (Fig. 10d). This clearly confirms the good stability of the sample during the photocatalytic process.

The efficiency of photocatalytic decomposition of fast green dye using  $\text{WO}_3$ -modified  $\text{TiO}_2$  polyscale crystals under both UV and sunlight irradiation is strongly determined by several factors. Mainly, the morphology of the as-prepared photocatalyst is tabular in shape with varied size ranging from 2 to  $>20 \mu\text{m}$  (Suzuki and Taga 2001). This type of structure is helpful in providing more active sites during photocatalysis and also favors the adsorption of dye molecules onto this photocatalyst which in turn are helpful in the photocatalytic process. Furthermore, in the  $\text{WO}_3$ -modified  $\text{TiO}_2$  polyscale crystals, a certain quantity of tungsten ions is doped into the crystal lattice  $\text{TiO}_2$  which was confirmed by XRD studies. Doping of tungsten ions into the crystal lattice of  $\text{TiO}_2$  facilitates in tuning the band energy of  $\text{TiO}_2$  such that  $\text{TiO}_2$  can be utilized as a photocatalyst under both

UV and visible light. Meanwhile,  $\text{WO}_3$  deposited onto  $\text{TiO}_2$  polyscale crystals forms an intimate contact forming heterojunction, thereby facilitating the free movement of photogenerated electrons from one semiconductor to another. Schematic diagram of charge transfer between  $\text{TiO}_2$  and  $\text{WO}_3$  heterojunction interface is presented in Fig. 11. Figure 11 clearly illustrates the moment of photogenerated electrons from  $\text{TiO}_2$  to  $\text{WO}_3$ . The photogenerated electrons transfer from conduction band (CB) of  $\text{TiO}_2$  to the CB of  $\text{WO}_3$ , whereas the photogenerated holes moves from the valence band (VB) of  $\text{WO}_3$  to the VB of  $\text{TiO}_2$ . During the flow of electrons from  $\text{TiO}_2$  to  $\text{WO}_3$ , the electrons are trapped by the active sites of  $\text{WO}_3$  where  $\text{W}^{6+}$  undergoes reduction forming  $\text{W}^{5+}$ . It is reported that the (101) facets of  $\text{TiO}_2$  are more reductive than (001) facets. During photocatalysis, the photogenerated electrons move toward (101) facets, where the (101) facets acts as a reservoir for these photogenerated electrons leading to the formation of highly reactive surface where the reduction of  $\text{O}_2$  takes place forming superoxide radicals (D'Arienzo et al. 2011; Tachikawa

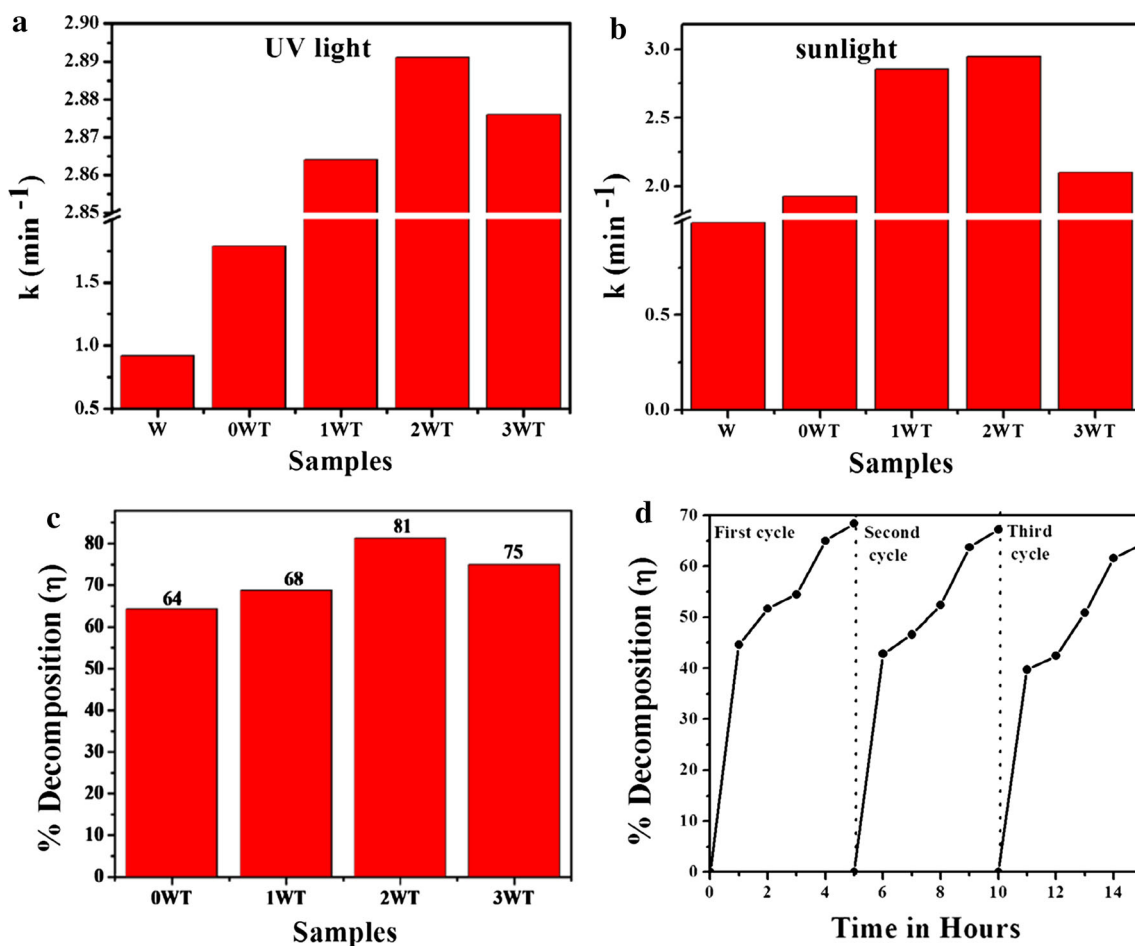


**Fig. 10** a, b Kinetic studies of FCF degradation under UV light and sunlight using W, 0WT, 1WT, 2WT and 3WT samples. c Comparison of the photocatalytic decomposition rate fast green dye using 0WT,

1WT, 2WT and 3WT samples under sunlight, d Cyclic decomposition rate curve for 2WT sample

**Table 2** Kinetic parameters obtained for the degradation of FCF under UV and sunlight using different samples

Samples	UV light		Sunlight	
	$k \times 10^2$ ( $\text{min}^{-1}$ )	$R^2$	$k \times 10^2$ ( $\text{min}^{-1}$ )	$R^2$
W	0.921	0.9995	0.987	0.9994
0WT	1.788	0.9980	1.926	0.9976
1WT	2.864	0.9936	2.856	0.9933
2WT	2.891	0.9930	2.946	0.9955
3WT	2.876	0.9933	2.103	0.9923

et al. 2011). Furthermore,  $\text{W}^{5+}$  combines with the superoxide radical and reoxidizes forming  $\text{W}^{6+}$ . This is a cyclic process due to which more and more electrons is recycled. These recycled electrons are beneficial in enhancing the lifetime of photogenerated electron–hole pair further leading to an increase in photocatalytic activity (Keller et al. 2003; Liqiang et al. 2006).

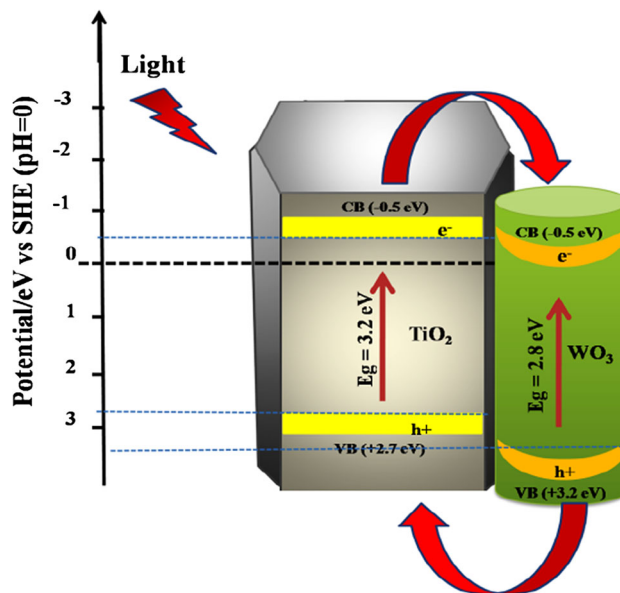


**Fig. 11** Schematic diagram of charge transfer between  $\text{TiO}_2$  and  $\text{WO}_3$  heterojunction interface



## Conclusion

Synthesis of WO<sub>3</sub>-modified TiO<sub>2</sub> polyscale crystals was carried out under mild hydrothermal condition. Our characterization studies clearly revealed that WO<sub>3</sub> has been deposited onto the TiO<sub>2</sub> polyscale crystals and a trace of them has been doped into the crystal lattice of TiO<sub>2</sub>. The photocatalytic degradation of fast green dye further proved that the reaction kinetics depend on various parameters such as light source, the concentration of semiconductor used and pH of the dye solution. We also observed that the efficiency of the photocatalyst depends on the added amount of WO<sub>3</sub> content. This is due to the change in the band gap of the semiconductor material and reduction in charge recombination. The prepared catalyst can be reused for a number of cycles, which will reduce the cost of operation. Moreover, the use of sunlight as the source of illumination in the photodegradation reaction could be a safe and highly cost-effective source. The reduction in COD of the dye solution suggests that the dye molecules were completely mineralized along with color removal. It can be concluded that WO<sub>3</sub>-modified TiO<sub>2</sub> polyscale crystal-assisted photocatalytic degradation of fast green dye is a versatile, economic, environmentally benign and efficient method of treatment, and can be used for degradation/removal of a wide variety of dyes and organics present in wastewater.

**Acknowledgements** The authors wish to thank all who assisted in this work.

## References

- Adhikari S, Sarkar D, Madras G (2015) Highly efficient WO<sub>3</sub>-ZnO mixed oxides for photocatalysis. *RSC Adv* 5(16):11895–11904
- Anpo M (1989) Photocatalysis on small particle TiO<sub>2</sub> catalysts. Reaction intermediates and reaction mechanisms. *Res Chem Intermed* 11:67–106
- Ashok CH, Rao VK, Shilpa Chakra CH (2016) CuO/TiO<sub>2</sub> metal oxide nanocomposite synthesis via room temperature ionic liquid. *J Nanomater Mol Nanotechnol* 05(01):12–15
- Boye B, Dieng MM, Brillas E (2002) Degradation of herbicide 4-chlorophenoxyacetic acid by advanced electrochemical oxidation methods. *Environ Sci Technol* 36:3030–3035
- Brown D, Hitz HR, Schgfer L (1981) The assessment of the possible inhibitory effect of dyestuffs on aerobic wastewater bacteria experience with a screening test. *Chemosphere* 10(3):245–261
- Che Ramli ZA, Asim N, Isahak WN, Emdadi Z, Ahmad-Ludin N, Yarmo MA, Sopian K (2014) Photocatalytic degradation of methylene blue under UV light irradiation on prepared carbonaceous TiO<sub>2</sub>. *Sci World J*. doi:10.1155/2014/415136
- D'Arienzo M, Carbajo J, Bahamonde A, Crippa M, Polizzi S, Scotti R, Wahba L, Morazzoni F (2011) Photogenerated defects in shape-controlled TiO<sub>2</sub> anatase nanocrystals: a probe to evaluate the role of crystal facets in photocatalytic processes. *J Am Chem Soc* 133(44):17652–17661
- Du X, Zhao J, Mi J, Ding Y, Zhou P, Ma B, Zhao J, Song J (2015) Efficient photocatalytic H<sub>2</sub> evolution catalyzed by an unprecedented robust molecular semiconductor{Fe11} nanocluster without cocatalysts at neutral conditions. *Nano Energy* 16:247–255
- El Saliby I, Shahid M, McDonagh A, Shon HK, Kim JH (2012) Photodesorption of organic matter from titanium dioxide particles in aqueous media. *J Ind Eng Chem* 18(5):1774–1780
- Ferraz MA, Möser S, Tonhaeuser M (1999) Control of atmospheric emissions of volatile organic compounds using impregnated active carbons. *Fuel* 78:1567–1573
- Griboval A, Gengembre P, Gengembre L, Payen E, Fournier M, Dubois JL, Bernard JR (1999) Hydrotreatment catalysts prepared with heteropolycompound: characterisation of the oxidic precursors. *J Catal* 188:102–110
- Grzechulska J, Morawski AW (2002) Photocatalytic decomposition of azo-dye acid black 1 in water over modified titanium dioxide. *Appl Catal B* 36:45–51
- Hamza A, Hampda M (1980) Multipurpose treatment of textile wastewater. In: *Proceedings of 35th Purdue industrial waste congress*, West Lafayette
- Jung HJ, Hong J, Suh JK (2013) A comparison of fenton oxidation and photocatalyst reaction efficiency for humic acid degradation. *J Ind Eng Chem* 19:1325–1330
- Kang JW, Hoffmann MR (1998) Kinetics and mechanism of the sonolytic destruction of methyl tert-butyl ether by ultrasonic irradiation in the presence of ozone. *Environ Sci Technol* 32:3194–3199
- Keller V, Bernhardt P, Garin F (2003) Photocatalytic oxidation of butyl acetate in vapor phase on TiO<sub>2</sub>, Pt/TiO<sub>2</sub>, and WO<sub>3</sub>/TiO<sub>2</sub> catalysts. *J Catal* 215(1):129–138
- Kung HH, Delmon B, Yates JT (1989) Transition metal oxides: surface chemistry and catalysis, studies in surface science and catalysis. Elsevier, Amsterdam, pp 292–293
- Leghari SAK, Sajjad S, Chen F, Zhang JI (2011) WO<sub>3</sub>/TiO<sub>2</sub> composite with morphology change via hydrothermal template-free route as an efficient visible light photocatalyst. *Chem Eng J* 166(3):906–915
- Li Y, Li L, Gong Y, Bai S, Ju H, Wang C, Xu Q, Zhu J, Jiang J, Xiong Y (2015) Towards full-spectrum photocatalysis: achieving a Z-scheme between Ag<sub>2</sub>S and TiO<sub>2</sub> by engineering energy band alignment with interfacial Ag. *Nano Res* 8(11):3621–3629
- Liao LF, Lien CF, Shieh DL, Chen MT, Lin JL (2002) FTIR study of adsorption and photoassisted oxygen isotopic exchange of carbon monoxide, carbon dioxide, carbonate, and formate on TiO<sub>2</sub>. *J Phys Chem B* 106(43):11240–11245
- Liqiang J, Yichun Q, Baiqi W, Shudan L, Baojiang J, Libin Y, Wei F, Honggang F, Jiazhong S (2006) Review of photoluminescence performance of nano-sized semiconductor materials and its relationships with photocatalytic activity. *Sol Energy Mater Sol Cells* 90(12):1773–1787
- Naeem K, Ouyang F (2013) Influence of supports on photocatalytic degradation of phenol and 4-chlorophenol in aqueous suspensions of titanium dioxide. *J Environ Sci* 25(2):399–404
- Nah YC, Ghicov A, Kim D, Berger S, Schmuki P (2008) TiO<sub>2</sub>-WO<sub>3</sub> composite nanotubes by alloy anodization: growth and enhanced electrochromic properties. *J Am Chem Soc* 130:16154–16155
- Nolan NT, Seery MK, Pillai SC (2009) Spectroscopic investigation of the anatase-to-rutile transformation of sol-gel-synthesized TiO<sub>2</sub> photocatalysts. *J Phys Chem C* 113(36):16151–16157
- Noorjahan M, Kumari VD, Subrahmanyam M, Boule PA (2004) A novel and efficient photocatalyst: TiO<sub>2</sub>-HZSM-5 combine thin film. *Appl Catal B* 47:209–213
- Ong WJ, Tan LL, Chai SP, Yong ST, Mohamed AR (2014) Facet-dependent photocatalytic properties of TiO<sub>2</sub>-based composites for energy conversion and environmental remediation. *ChemSusChem* 7(3):690–719



- Ong WJ, Tan LL, Chai SP, Yong ST (2015) Heterojunction engineering of graphitic carbon nitride (g-C<sub>3</sub>N<sub>4</sub>) via Pt loading with improved daylight-induced photocatalytic reduction of carbon dioxide to methane. *Dalton Trans* 44(3):1249–1257
- Ong WJ, Putri LK, Tan LL, Chai SP, Yong ST (2016) Heterostructured AgX/g-C<sub>3</sub>N<sub>4</sub> (X = Cl and Br) nanocomposites via a sonication-assisted deposition-precipitation approach: emerging role of halide ions in the synergistic photocatalytic reduction of carbon dioxide. *Appl Catal B* 180:530–543
- Rajeshwar K, Osugi M, Chanmanee W, Chenthamarakshan CR, Zaroni MVB, Kajitvichyanukul P, Krishnan Ayer R (2008) Heterogeneous photocatalytic treatment of organic dyes in air and aqueous media. *J Photochem Photobiol. C* 9:171–192
- Safaei E, Mohebbi S (2016) Photocatalytic activity of nanohybrid Co-TCPP@TiO<sub>2</sub>/WO<sub>3</sub> in aerobic oxidation of alcohol under visible light. *J Mater Chem A* 4(10):3933–3946
- Sajan CP, Shahmoradi B, Shivaraju HP, Rai KML, Ananda S, Shayan MB, Thonthai T, Rao GVN, Byrappa K (2010) Photocatalytic degradation of textile effluent using hydrothermally synthesised titania supported molybdenum oxide photocatalyst. *Mater Res Innov* 14(1):89–94
- Sayama K, Hara K, Mori N, Satsuki M, Suga S, Tsukagoshi S, Abe Y, Sugihara H, Arakawa H (2000) Photosensitization of a porous TiO<sub>2</sub> electrode with merocyanine dyes containing a carboxyl group and a long alkyl chain. *Chem Commun (Camb)*. doi:10.1039/b001517m
- Souther RH, Alspaugh TA (1957) Textile wastes recovery and treatment. *Sew Ind Wastes* 9(8):918–935
- Stock NL, Peller J, Vinodgopal K, Kamat PV (2000) Combinative sonolysis and photocatalysis for textile dye degradation. *Environ Sci Technol* 34:1747–1750
- Su D, Wang J, Tang Y, Liu C, Liu L, Han X (2011) Constructing WO<sub>3</sub>/TiO<sub>2</sub> composite structure towards sufficient use of solar energy. *Chem Commun (Camb)* 47(14):4231–4233
- Suzuki M, Ito T, Taga Y (2001) Photocatalysis of sculptured thin films of TiO<sub>2</sub>. *Appl Phys Lett* 78(25):3968
- Tachikawa T, Yamashita S, Majima T (2011) Evidence for crystal-face-dependent TiO<sub>2</sub> photocatalysis from single-molecule imaging and kinetic analysis. *J Am Chem Soc* 133(18):7197–7204
- Vannice MA (1982) Titania-supported metals as CO hydrogenation catalysts. *J Catal* 74:199–202
- Wachs IE, Saleh RY, Chan SS, Chersich CC (1985) The interaction of vanadium pentoxide with titania (anatase): part 1. Effect on O-xylene oxidation to phthalic anhydride. *Appl Catal B* 15:339–352
- Wainwright MS, Foster NR (1979) Catalysts, kinetics and reactor design in phthalic anhydride synthesis. *Catal Rev* 19(2):211–292
- Wang HL, Lewis JP (2005) Effects of dopant states on photoactivity in carbon-doped TiO<sub>2</sub>. *J Phys: Condens Matter* 17(21):L209–L213
- Xiong Z, Zhao XS (2012) Nitrogen-doped titanate-anatase core-shell nanobelts with exposed {101} anatase facets and enhanced visible light photocatalytic activity. *J Am Chem Soc* 134(13):5754–5757

